Journal of Environmental Pathology, Toxicology and Oncology, 20(Suppl. 1):119–132 (2001)

Reactivity of Free Radicals on Hydroxylated Quartz Surface and Its Implications for Pathogenicity of Silicas: Experimental and Quantum Mechanical Study

Robert Konecny, Steve Leonard, Xianglin Shi, Victor Robinson, & Vincent Castranova*

We studied the adsorption of hydroxyl radicals and superoxide anion radicals on a hydroxylated α-quartz surface using cluster and periodic slab models by means of density functional calculations. Models of two hydroxylated α-quartz surfaces—(0001) and $(01\bar{1}1)$—have been used in the simulations. The hydroxyl radical adsorbs readily on both surfaces. The subsurface Si–O bonds are weakened during the adsorption resulting in surface layer destabilization. This destabilization leads directly to surface disintegration in the case of •OH/$(01\bar{1}1)$ adsorption. The product of the surface disintegration and reconstruction is a surface terminated by silanol groups (Si–OH) and siloxyl radicals (Si–O•). The model calculations suggest that adsorption of •OH on a hydroxylated quartz surface transforms a chemically inert, aged, silanol terminated surface to a very reactive, silicon-based radical terminated surface. The activated surface may then cause oxidative damage to the adsorbed biomaterial.

The superoxide anion radical adsorbs on both surfaces, but the adsorption products are only weakly bonded to the surface. The calculated energy barrier for the $O_2^{\bullet-}$ activated subsurface Si–O bond dissociation is 10 kcal/mol, which is higher than for the •OH activated process (4 kcal/mol). The calculated weaker bonding to the surface and higher activation energy barrier suggest that the superoxide anion radical will be less efficient in reactivation of an aged, hydroxylated quartz surface than the hydroxyl radical. The importance of the specific geometry of the surface silicon atoms on the surface reactivity and adsorption properties is also discussed. The theoretical predictions are supported experimentally using chemiluminescence to monitor reactivation of the aged silica surface by superoxide anion radicals.

KEY WORDS: *ab initio* calculations, silicosis, quartz, surface radicals

Introduction

Exposure to silica dust, as one of the major occupational and environmental hazards, has been associated with pulmonary fibrosis, alveolar proteinosis, and autoimmune diseases. It has also been recently linked with the development of lung cancer.[1] Although silicosis has been the subject of numerous

National Institute for Occupational Safety and Health, Morgantown, WV. *Current address: Keck Center, University of California San Diego, La Jolla. Correspondence: Vincent Castranova, Ph.D., National Institute for Occupational Safety and Health, 1095 Willowdale Rd., Morgantown, WV 26505-2888; VCastranova@cdc.gov.

Acknowledgments: The authors wish to thank William E. Wallace and Sid Soderholm for stimulating and fruitful discussions and NIOSH for the research opportunity.

0731-8898/01/$5.00

studies for more than 40 years, the molecular mechanism of the process is still not very well understood. Silicosis arises from complex interactions between biological macromolecules and cells on one side and a silica surface on the other. The complexity and number of factors involved in these multistep interactions is one of the reasons why the mechanism of silica toxicity has been eluding detailed description. Furthermore, the lack of homogeneous, well-characterized surface structure of respirable dust particles, together with the enormous structural complexity of silicas, makes experimental determination of the mechanism particularly difficult. Quantum-chemical modeling, with its accuracy and insight at the atomic level, can shed some additional light on the individual steps in this complex interaction mechanism. Because of the recent advances in methodology and algorithm solving techniques, *ab initio* simulations have become an excellent complementary tool to experiment.

It is generally accepted[2-8] that one of the major contributors to the pathogenesis of silicosis is oxidative stress from both surface and cell-derived oxidant species. Surface-derived oxidants, such as free radical and peroxides, may also inflict direct damage on the epithelial cells. Among these surface-derived oxidants, free radicals and particularly hydroxyl radicals (•OH) have been shown to play a major role.[3,5-7,9-16] This is not surprising, since the hydroxyl radical reaction with biomolecules has been shown to have deleterious effects on biological systems. However, despite extensive experimental work on the role of free radicals in silica toxicity, a complete understanding of the mechanism of interaction between these free radicals and the surface is lacking.

Crystalline silica, with the chemical unit formula SiO_2, is one of the most common materials on earth. It exists in several different polymorphic forms with α-quartz being the most common and also one of the most toxic.[17] In all forms of silica, except stishovite, the silicon atoms are surrounded by an approximately tetrahedral array of oxygen atoms. Each oxygen atom is bonded to two silicon atoms and serves to link the tetrahedra. When bulk crystalline silica is cut and a surface is formed, the Si–O bonds at the cleavage are ruptured (Schema 1). The Si–O bond separation is primarily homolytic due to the dominant covalent character of the bond. This leaves an unpaired electron on both the Si and O atoms. Thus, the newly created surface consists of >Si• and >Si–O• radical species (the > label represents bonding to the bulk of the crystal).

These reactive surface radicals are able to generate hydroxyl radicals in an aqueous environment via the Fenton mechanism in the presence of transition metal ions (e.g., iron).[6,7,10,15] Other mechanisms of free radical release have been proposed as well.[18-20] The formed hydroxyl radicals are highly reactive species capable of causing oxidative damage to biomaterial adsorbed on or in the near vicinity of the silica surface. Because of its reactivity in an aqueous environment or in the presence of water vapor, the surface silicon radicals will be transformed over a period of time to fairly unreactive silicon bonded hydroxyl groups, silanols (Si–OH). Thus, the amount of generated hydroxyl radicals will be larger on freshly fractured silica surfaces where the concentration of surface silicon radicals is higher. As a corollary, the ability to generate hydroxyl radicals on the aged, silanol-terminated silica surface should be diminished. However, there is experimental evidence suggesting that the aged silica surface is still able to produce hydroxyl radicals although to a much lesser extent than the freshly fractured surface.[3,6,15,21] Others have also experimentally shown that the silicon-based radicals Si• and SiO• are still present in aged ground silicas, although it is not clear if they are located at the surface or in subsurface layers.[9,12,13,22]

Previous theoretical work employing a simple cluster model of the surface[23] predicted that adsorption of hydroxyl radicals on aged, silanol-terminated

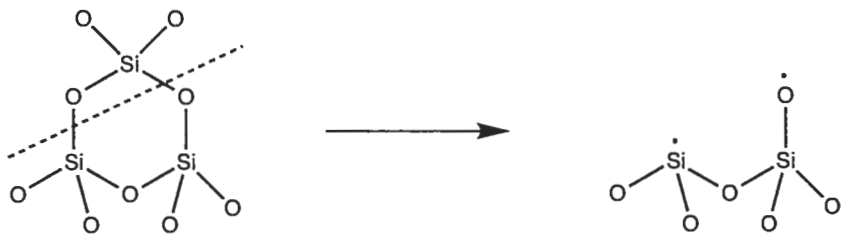

Schema 1

quartz surface may lead to disintegration of the surface layer and reactivation of the surface in the chemical reactivity sense. The hydroxyl radical induced quartz surface structural changes may produce surface silicon-based radicals, which can then participate in other chemical and biological interactions. The calculation predicted that when •OH adsorbs on a hydroxylated quartz surface, it forms a 5-coordinate surface silicon complex in which Si–O subsurface bonds are weakened. These bonds are susceptible to dissociation, which may lead to surface dissolution. The calculated energy barrier for this process is only 4 kcal/mol, which is significantly lower than the estimated barrier in the rate determining step for OH^- catalyzed quartz surface dissolution (19 kcal/mol).[24] Consequently, •OH radicals may be able to transform a chemically fairly inert, silanol-terminated, aged quartz surface to a reactive surface containing silicon-based radicals.

The results of the theoretical calculations[23] also suggested that the local geometry of surface silicon atoms and silanol groups may effect reactivity of these surface sites towards hydroxyl radicals. The surface silanols are experimentally observed in two local configurations (see Schema 2).[25-27] In the isolated single silanol (a) only one hydroxyl is bonded to the surface silicon atom, whereas in the geminal silanols (b) there are two hydroxyls attached to the same surface Si. The other surface silicon valences are saturated by binding to the bulk crystal, represented as Si_b and O_b in Schema 2a and 2b. These two distinct silanol configurations will interact to a different degree with different surface adsorbents.

This combined theoretical and experimental study is a continuation of our previous effort to understand the reactivity of hydroxyl radical species on hydroxylated quartz surfaces. In this work, we have extended our modeling using three-dimensional periodic slab models that allow for a more accurate description of surface properties and reactivity. In addition to the hydroxyl radical, we have also studied the interaction of another biologically important radical species, the superoxide anion radical, with the hydroxylated quartz surface using both cluster and slab surface models. The theoretical predictions have been tested experimentally using chemiluminescence techniques.

Computational Methods

Modeling of periodic systems and surfaces in particular still poses a variety of challenges. There are two fundamental approaches to approximate the real surface—either by using a cluster model of the surface or a three dimensional periodic slab model. Both approximations have strengths and weaknesses which need to be taken into account when applying quantum chemical methods to these models. In the cluster approach, only a limited number of atoms around the active surface site is considered. This procedure of cutting out the cluster from the solid inevitably creates structural artifacts at the border of the cluster, which must be dealt with in the subsequent calculation. However, the relatively small size of the cluster allows for very accurate calculations, although the predictions based on these calculations are limited only to localized events at the surface active site.

In the other approach, the periodic treatment employs a slab of the crystal consisting of several layers of the material. To simulate a surface, the slab is terminated at the top and bottom by a vacuum layer. This unit cell is infinitely repeated in all three dimensions. Although quite computationally demanding, the periodic slab model approach provides reliable predictions of surface properties, including long range surface and surface/adsorbate interactions.

We employed both approximations in our study, which allowed us to gain comprehensive insight into the reactivity of hydroxylated quartz surfaces.

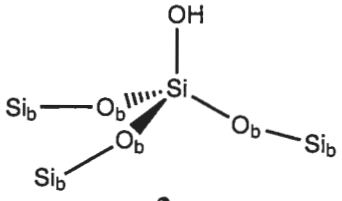

2a

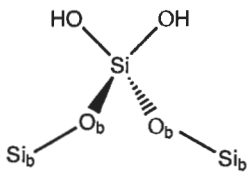

2b

Schema 2

Cluster Models

The two cluster models used in our calculations consist of a center silicon atom approximating the surface silicon, one or two hydroxyl groups attached to the silicon atom and three or two $OSiH_3$ groups modeling the subsurface bonding. These two clusters represent surface sites with isolated silanols and geminal silanols, respectively (see Schema 3).

The calculations have been performed using the hybrid B3LYP exchange-correlation functional (DFT).[28,29] The 6-31G** Gaussian basis set was employed with polarization on heavy elements and hydrogen atoms. All degrees of freedom of the studied systems were optimized. Several unidimensional potential energy surface scans were performed using a single geometrical constraint–bond distance. A transition state search was carried out using the Berny algorithm.[30] All stable points on the potential energy surface have been verified by full frequency analysis. The calculations were carried out using the Gaussian98 package.[31]

Periodic Slab Models

The slab models were prepared by repeating O–Si–O layers along either the (0001) or (01$\bar{1}$1) direction. The (0001) and (01$\bar{1}$1) labels represent directions (in hexagonal coordinates) in which the crystal is cut to create the surface. The slabs consist of 9 SiO_2 monolayers, with the unsaturated silicon atom valencies at the bottom terminated by hydrogen atoms, and a vacuum region. The convergence of the total energy with respect to the size of the vacuum layer was checked. A 15-Å vacuum layer was used in calculations involving hydroxyl radicals. Because the unit cell containing the superoxide anion radical and the quartz surface has a negative charge, the total energy of the systems diverges with increased size of the vacuum layer due to augmentation of the electrostatic contribution. In this case, we set the depth of the vacuum region at 21 Å, which prevented spurious interactions between the slabs. The calculated relative adsorption energies for the charged unit cell should be considered only approximate. Although no ion–ion screening between the anion in one unit cell and the neighboring cells was employed, the error resulting from this effect is only about 1.3 kcal/mol per adjacent unit cell.

The (0001) and (01$\bar{1}$1) cleavages were chosen as representative of a typical α-quartz surface, because they form one of the most energetically stable surfaces upon hydroxylation. The optimized geometries of the hydroxylated surfaces are presented in Figs. 1 and 2 and important structural parameters are in Table 1.

The periodic slab calculations were carried out using the Vienna *ab initio* simulation package (VASP)[32-35] within the local density approximation (LDA) to density functional theory.[36,37] The fully nonlocal optimized ultrasoft pseudopotentials were used.[38,39] The optimization of the atomic geometry was performed via a conjugated-gradient minimization of the total energy with respect to the atomic coordinates. Brillouin-zone integrations were performed using a $3 \times 3 \times 1$ grid of Monkhorst-Pack special points[40] and the linear tetrahedron method[41] with the corrections proposed by Blöchl et al.[42] Several test calculations have been carried out to determine the optimal number of irreducible *k*-points.

All the adsorption product optimizations were performed using a 1×1 surface unit cell at 1.0 monolayer adsorbent coverage—that is, there was one molecule of adsorbent per surface silicon. This approximation significantly reduces computational cost.

Experimental Methods

Freshly fractured crystalline silica exhibits Si-O• and Si• radicals on the cleavage planes. The existence

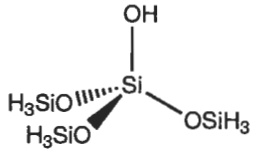

3a

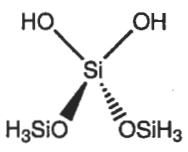

3b

Schema 3

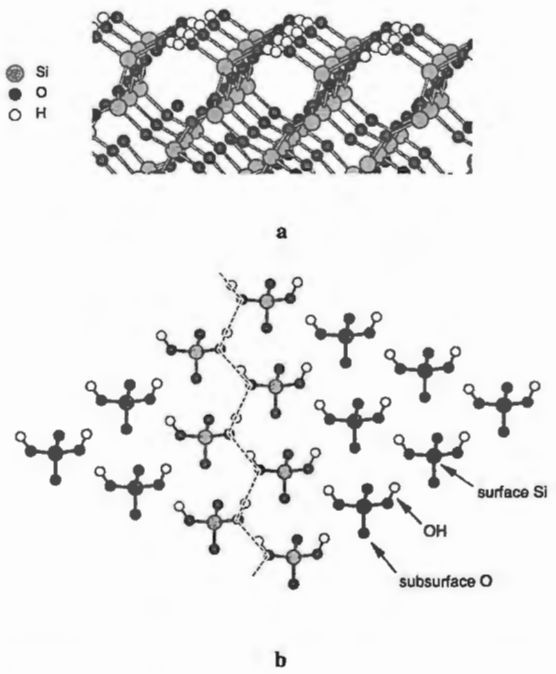

FIGURE 1. Optimized geometry of the hydroxylated (0001) α-quartz surface. Panel a: side view of surface. Panel b: top view of surface first layer, zig-zag hydrogen-bonded surface silanols depicted. Surface sublayers are omitted from this panel for clarity. This and the following slab model figures comprise several surface unit cells cut from the infinite slab used in our calculation. There is always one molecule of adsorbent per surface silicon atom (i.e., adsorption is modeled at 1.0 monolayer coverage).

of such surface radicals has been verified by electron spin resonance (ESR) spectroscopy.[10] Freshly ground silica also generates energy that can be measured as chemiluminescence.[43] Both the ESR and chemiluminescence signals of fresh silica decay with time

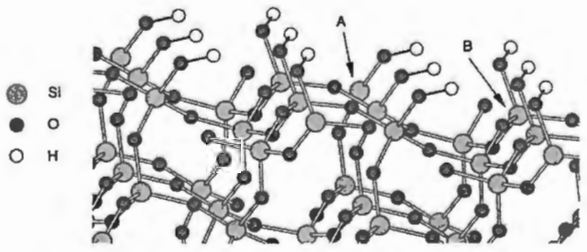

FIGURE 2. Optimized slab model geometry of the hydroxylated (01$\bar{1}$1) α-quartz surface. Two geometrically distinct silicon atom surface sites, A and B, are shown.

TABLE 1. Calculated Structural Data of Hydroxylated (0001) and (01$\bar{1}$1) α-Quartz Surface (First Surface Layer Only) Using Periodic Slab Model

	(0001)	(01$\bar{1}$1)
r(Si–OSi)	1.608[a]	1.606[a]
r(Si–OH)	1.606, 1.639	1.598, 1.633
α(Si–O–Si)	143.2[a]	142.2[a]

Note: Bond lengths in Å and bond angles in degrees.
[a] Average value.

after grinding. The $T_{1/2}$ for decay of the ESR signal is approximately 30 hours in air, while the $T_{1/2}$ for decay of the chemiluminescence signal is approximately 28 minutes in buffered medium.

In the present investigation, the refreshening of an aged silica surface by superoxide anion radicals was monitored by measuring chemiluminescence. Superoxide radicals were generated by the reaction of xanthine (1 mM) and xanthine oxidase (20 μM). The crystalline silica sample (0.05 g/mL or 0.1 g/mL) used was Min-U-Sil (US Silica, Berkeley Springs, WV, USA). X-ray spectrometric analysis indicated that 98.5% of the particles were crystalline silica, with 99% of the particles having a diameter <5 μm. Chemiluminescence (CL), measured as counts per minute (cpm), was determined using an automated luminometer (Berthold Autolumat LB953; Wallac, Gaithersburg, MD, USA). CL of HEPES-buffered samples (145 mM NaCl, 5 mM KCl, 0.008 mg % luminol, and 10 mM HEPES; pH 7.4) in the absence or presence of xanthine/xanthine oxidase or silica, respectively, was monitored at 42 °C for 45 minutes. Data were plotted as cpm versus time and the curves integrated to obtain total CL in cpm over the 45-minute measurement period. Data are presented as percent of control (means ± standard errors of 4–5 experiments). Differences between test and control were determined using original cpm data by one-way ANOVA, followed by multiple comparisons among means using Tukey-Kramer's Honestly Significant Difference test. Two-way ANOVA was used to evaluate non-addition interaction of the superoxide generation system and silica treatments. Significance was set at $p \leq 0.05$.

Results and Discussion

Interaction of Hydroxyl Radical with Surface–Slab Model Calculations

To verify our earlier prediction on the reactivity of •OH with the quartz surface and to gain further insight into this process, we studied the interaction of hydroxyl radicals with the surface using the three-dimensional periodic slab model.

We employed slab models of two stable hydroxylated quartz surfaces, (0001) and (01$\bar{1}$1) cleavages. These surfaces have quite different configurations of the surface hydroxyl groups, silanols. Whereas the (0001) surface contains only geminal silanols (Fig. 1), the (01$\bar{1}$1) surface is terminated by isolated silanols (Fig. 2). Thus, the silicon reactive sites on these two surfaces are in two different chemical and geometrical environments. This is reflected, for instance, in the ability of silanols on these surfaces to interact with neighboring silanol groups. The geometrical configuration of the surface silicon atoms and geminal silanols on the (0001) plane provides a favorable environment for extensive hydrogen bonding. The hydrogen bonded geminal silanols form infinite zig-zag OH—OH chains on the surface (Fig. 1b). Because of geometrical constraints, the (01$\bar{1}$1) surface silanols can only participate in limited hydrogen bonding—only two adjacent silanols can interact—and the silanols form small, hydrogen-bonded clusters on the surface (Fig. 2). The different extent of silanol hydrogen networking on these two surfaces will modulate to some extent the surface reactivity and adsorption properties.

There is also a difference in steric requirements at the silicon atom surface sites on these two different cleavages. The two relatively small geminal silanol groups at the surface silicon atom on the (0001) surface present a sterically open environment for the incoming adsorbent molecule. On the other hand, the surface Si atoms at the (01$\bar{1}$1) plane are in a more sterically crowded environment being bonded to three bulky –OSi groups and only one small OH group. Therefore, an adsorbing •OH encounters stronger repulsive interaction at the isolated silanol surface site than at the geminal site. Also, the geminal silanol group involvement in the extensive hydrogen bonding forces the OH groups to bend closer to the surface, exposing the surface silicon atom to the adsorbing molecule (Fig. 1).

Although the (01$\bar{1}$1) surface contains isolated silanols only, there are two geometrically distinct surface silicon sites, A and B (Fig. 2). While the surface silicon site A has two Si–OSi bonds in the surface plane, and one of the Si–OSi bonds is perpendicular to the surface, site B has all three Si–OSi bonds approximately coplanar with the surface plane. In other words, the plane created by three corners of the SiO_4 tetrahedra (surface Si being at the center of the tetrahedra) is nearly coplanar with the surface plane at site B but is almost perpendicular to the surface plane at site A. These subtle structural differences influence the extent of the interaction between the adsorbent molecule and the surface site.

We performed geometry optimization of the •OH adsorption product on both the (0001) and (01$\bar{1}$1) surfaces. To simulate •OH interaction with hydroxylated (0001) quartz surface, we started geometry optimization from a structure where •OH is near the surface (Fig. 3a). During the energy minimization the •OH desorbed from the surface and formed a bond between its oxygen atom and the hydrogen of one of the surface silanol groups. The hydroxyl radical eventually abstracted the silanol hydrogen atom, forming a water molecule and leaving the siloxyl radical (Si–O•) on the surface. This water molecule stayed near the surface, hydrogen bonded to the surface silanol. The hydroxyl radical interaction with (0001) quartz surface produces siloxyl radicals (si–O•) on the surface. The hydroxyl radical is initially adsorbed on the surface and forms a bond to the surface silicon atom. As the simulation progressed, the hydroxyl radical/surface silicon attractive interaction was weakened and eventually replaced by stronger interaction between the •OH and hydrogen atom on one of the surface geminal silanols. This interaction led to hydrogen abstraction from the silanol group and formation of a water molecule and a siloxyl radical on the surface. The calculated reaction energy for the overall process is –24.2 kcal/mol per unit cell, the reaction is thermodynamically favorable. The structures of the starting and optimized geometry are shown in Fig. 3 and structural data are presented in Table 2.

Adsorption of •OH on the (01$\bar{1}$1) surface leads to a dramatically different result than on the (0001) surface. We have optimized geometry of the product of this adsorption starting from the optimized hydroxylated (01$\bar{1}$1) surface with two •OH molecules attached to two surface silicon sites (A and B) per unit cell (Fig.

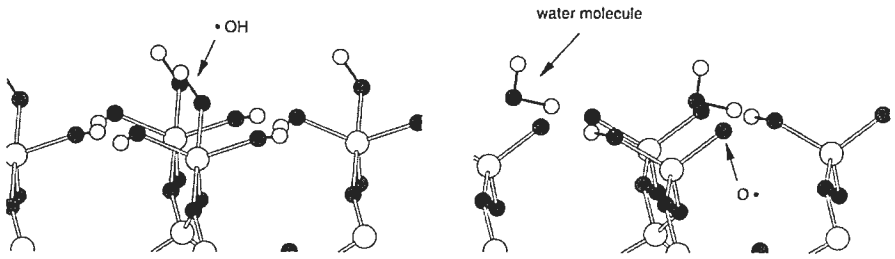

FIGURE 3. Starting (a) and optimized (b) structure of hydroxylated (0001) α-quartz surface with adsorbed •OH radicals. The hydroxyl radical abstracts a hydrogen atom from one of the surface silanols, forming a water molecule and a siloxyl radical (Si–O•) on the surface. Several surface unit cells are shown.

4a). During the optimization, the two hydroxyl radicals formed strong bonds with the surface silicons, while some of the Si–O subsurface bonds weakened. This bond weakening eventually led to the rupture of the Si–O bond at one of the surface silicon sites (site A) during the minimization. The calculated product of the adsorption is shown in Fig. 4b. The overall reaction energy for the •OH adsorption and surface reconstruction is −62.4 kcal/mol per •OH molecule and unit cell. This striking result suggests that although •OH interacts to a large degree with both surfaces, the mechanism of these interactions is quite different. The fact that we have observed the subsurface bond rupture during the •OH/(01$\bar{1}$1) energy minimization calculation implies that this process, starting from the •OH adsorption and leading to the subsurface Si–O bond breaking, is energetically downhill and does not encounter a significant energy barrier along the reaction pathway. It is also interesting to note that the actual subsurface Si–O bond breaking occurs at site A and not B. This suggests that site A is more reactive than site B, probably because of a more strained geometry at site A. Also, it is quite possible that a hydroxyl radical is able to abstract a hydrogen atom from the surface silanol group on the (01$\bar{1}$1) surface, as it does on the (0001) surface. Although we did not ob-

TABLE 2. Calculated Structural Data for (0001) and (01$\bar{1}$1) Hydroxylated α-Quartz Surface with Adsorbed •OH [Geometries at Sites A and B on (01$\bar{1}$1) Surface Reported Separately]

		•OH/(01$\bar{1}$1)	
	•OH/(0001)	A	B
r(Si–OSi)[a]	1.595	1.612, 1.620	1.600, 1.603
r(Si–OSi)[b]	1.603	1.615	1.613
r(Si–OH)	1.617,[c] 1.629	1.500, 1.598	1.634, 1.653
α(HO–Si–O)[a]		68.4, 78.3	65.2, 80.9
α(HO–Si–O)[b]		176.7	167.7

Note: Bond lengths in Å and bond angles in degrees.
[a] *cis*, next to adsorbate (•OH).
[b] *trans*, on opposite side to adsorbate.
[c] Siloxyl Si–O• bond length.

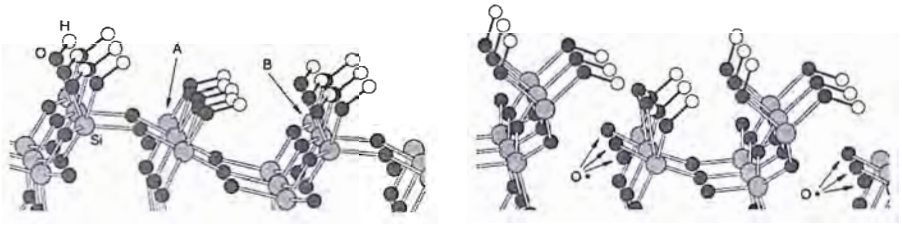

a b

FIGURE 4. Starting (a) and optimized (b) structure of hydroxylated $(01\bar{1}1)$ α-quartz surface with adsorbed •OH radicals. Each surface silicon atom is in a 5-coordinate configuration, connected to three oxygen atoms (surface and subsurface atoms), one silanol group, and one adsorbed hydroxyl radical. Adsorption of hydroxyl radicals on hydroxylated surface destabilizes surface and results in surface disintegration and reconstruction. Location of newly formed siloxyl radicals (Si–O•) is shown. Also two silicon atom surface sites A and B are shown.

serve the silanol hydrogen abstraction on the $(01\bar{1}1)$ surface during our calculation, we cannot rule it out as a possible reaction pathway, because we did not scan the full potential energy surface.

We also note that although the calculations were carried out in vacuum, the presence of a polar solvent (e.g., water) in the real environment is not expected to significantly alter predicted reaction energetics for these neutral radical reactions.[44]

In summary, although the •OH initially adsorbs on both surfaces, it destabilizes the $(01\bar{1}1)$ surface to a much larger extent, eventually inducing considerable surface reconstruction and formation of a silicon-based radical terminated surface. The predicted different magnitude of interaction at sites A and B on the $(01\bar{1}1)$ surface also emphasizes the role of the local surface site configuration in the overall silica surface reactivity.

Interaction of Superoxide Anion Radical with the Surface

Cluster Model Calculations

To study the interaction of the superoxide radical anion ($O_2^{\bullet-}$) with the surface in detail, we have employed a cluster model of the surface. The $O_2^{\bullet-}$ reacts with the geminal silanol cluster model forming a pentacoordinated silicon complex, **4**. The calculated reaction energy of the process is −52.3 kcal/mol. The optimized geometry of the complex **4** is presented in Fig. 5 and structural data in Table 3. The adsorbed superoxide radical in **4** is positioned *cis*, next to one $OSiH_3$ group, and *trans*, opposite the other $OSiH_3$ group. The *trans*-coordinated $OSiH_3$ group becomes less strongly bonded upon $O_2^{\bullet-}$ adsorption, which is reflected in the longer *trans*-Si–$OSiH_3$ distance (1.81 Å) compared to the *cis*-Si–$OSiH_3$ bond length (1.71 Å). This weaker, destabilized *trans*-Si–$OSiH_3$ bond will undergo dissociation much easier than will the *cis*-Si–$OSiH_3$ bond.

We have also considered the interaction between a superoxide radical and the silicon atom in the isolated silanol cluster model. The $O_2^{\bullet-}$ reacts with the cluster with its two oxygen atoms simultaneously attaching to the center Si and to the silicon atom in one of the $OSiH_3$ groups. The resulting complex **5** is depicted in Fig. 5. The adsorption energy for this process is −57.5 kcal/mol. However, the formation of this adsorption complex is an artifact of our cluster model, since this configuration is not possible on the real surface. The simultaneous bonding of superoxide oxygens to two surface silicon atoms is unlikely because of geometrical constraints—the distance between two Si atoms on the real surface is too large for this interaction to occur.

To estimate an energy barrier to the *trans*-Si–$OSiH_3$ bond dissociation in **4**, which would correspond to the subsurface Si–O bond rupture on the real surface, we have located a transition state structure on this reaction pathway. A transition state on a potential energy surface corresponds to a local energy maximum along the reaction coordinate. This energy maximum represents an activation energy needed for a reaction to occur. The optimized tran-

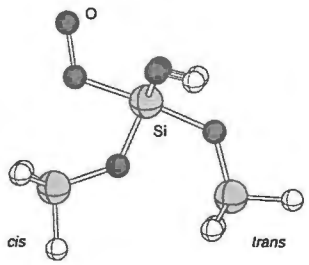

4

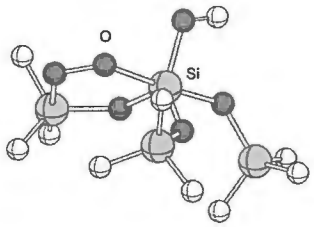

5

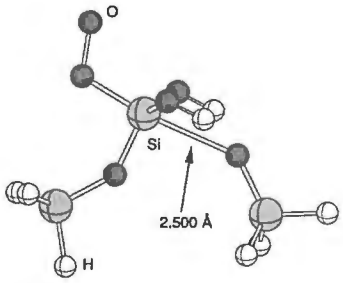

6

FIGURE 5. Calculated products of O_2^- adsorption on geminal (**4**, *cis* and *trans* $OSiH_3$ groups are labeled) and isolated (**5**) silanol cluster model. Optimized transition state geometry **6** for superoxide radical activated Si–$OSiH_3$ bond dissociation from **4** is also shown. Elongated Si–O bond being ruptured in **6** is marked.

sition state geometry **6** is shown in Fig. 5, with relevant structural parameters in Table 3. The calculated energy barrier to the Si–O bond dissociation in the cluster model **4** is 10.3 kcal/mol. This barrier is higher than the predicted barrier for the •OH activated process (4 kcal/ mol), but it is still lower than

TABLE 3. Optimized Cluster Model Structural Parameters for Product (**4**) and Transition State Geometry (**6**) of Superoxide Adsorption on Hydroxylated Quartz Surface

	4	6
r(Si–OO)	1.842	1.763
r(Si–OH)	1.682, 1.682	1.639, 1.638
r(Si–$OSiH_3$)	1.710, 1.811	1.659, 2.501
α(OO–Si–OH)	90.8, 90.8	103.2, 103.7
α(HO–Si–OH)	122.1	120.3
α(OO–Si–$OSiH_3$)	85.3, 175.3	96.0, 172.8
α(H_3SiO–Si–$OSiH_3$)	90.0	91.3
α(Si–O–SiH_3)	132.6, 128.3	141.4, 139.8

Note: Bond lengths in Å and bond angles in degrees.

the calculated energy barrier in the rate determining step in the OH^- catalyzed quartz surface dissolution (19 kcal/mol).[24] These results suggest that the $O_2^{\bullet-}$ activated Si–O subsurface bond dissociation, although still energetically favorable, will occur less likely than when activated by hydroxyl radicals. Thus, superoxide anion radicals will be less efficient in disintegration and reactivation of aged, silanol-terminated quartz surface than hydroxyl radicals.

Slab Model Calculations

To investigate the role of the bulk silica crystal on the $O_2^{\bullet-}$ surface adsorption, we have geometry optimized the product of the reaction using a three-dimensional periodic slab model. Again we have looked at adsorption on two stable hydroxylated α-quartz surfaces, (0001) and (01$\bar{1}$1).

The superoxide radical adsorbs on both of these cleavages although to a different degree. When adsorbing on the (0001) surface, $O_2^{\bullet-}$ forms only a weak bond to the surface silicon atom (Fig. 6, Table 4). The bonding energy between the surface and $O_2^{\bullet-}$ is −4.5 kcal/mol per unit cell. The Si–OO bond distance is quite long (2.13 Å) compared to the Si–OO bond length in the cluster model 4 (1.84 Å) (Table 3). This is also indicative of a weak interaction. As can be seen in Table 4, the adsorbed $O_2^{\bullet-}$ again destabilizes the surface layer, the subsurface Si–O bonds are elongated (compared to the bare hydroxylated quartz surface), and the *trans*-Si–O bond is weakened the most.

When $O_2^{\bullet-}$ interacts with the (01$\bar{1}$1) cleavage, superoxide radical adsorption proceeds in a local surface geometry dependent manner. Our calculations suggest that the superoxide radical adsorbs at site A but does not form a stable product at site B. This is most likely due to a more sterically hindered coordination space at site B. Consequently, $O_2^{\bullet-}$ can be adsorbed only at half of the silicon surface sites, compared to the (0001) surface. The starting adsorbate/surface geometry is shown in Fig. 7a, and the optimized, minimum energy structure is presented in Fig. 7b. The relevant structural data are in Table 4. In the final geometry, one $O_2^{\bullet-}$ molecule desorbs from the surface (at site B); the other is bonded to the surface (at site A). The bonding energy between the adsorbed $O_2^{\bullet-}$ and the surface is −12.6 kcal/mol per unit cell, suggesting only a weak bond. This is also indicated by the longer Si–OO distance (2.08 Å) compared with the Si–OO bond length in the cluster 4 (1.84 Å).

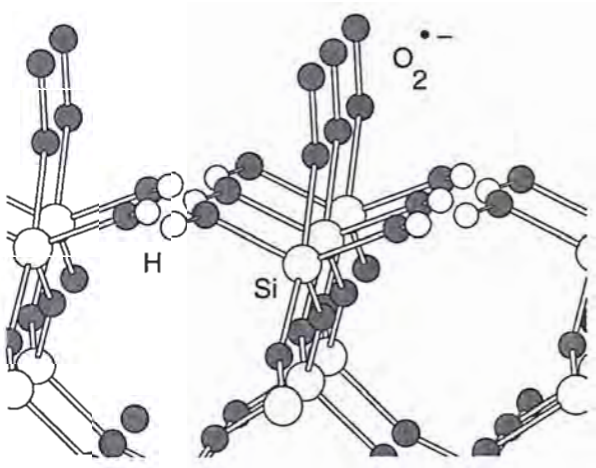

FIGURE 6. Optimized slab model geometry of $O_2^{\bullet-}$ interaction with hydroxylated (0001) α-quartz surface. Superoxide anion radical is weakly adsorbed on surface (positioned perpendicularly to surface). Hydrogen bonding between surface silanols is retained.

TABLE 4. Calculated Structural Data for (0001) and (01$\bar{1}$1) Hydroxylated α-Quartz Surfaces with Adsorbed $O_2^{\bullet-}$ [Geometries at Sites A and B on (01$\bar{1}$1) Surface Reported Separately]

		$O_2^{\bullet-}$/(01$\bar{1}$1)	
	$O_2^{\bullet-}$/(0001)	A	B
r(Si–OSi)[a]	1.625	1.610, 1.646	1.580, 1.609, 1.640
r(Si–OSi)[b]	1.694	1.720	
r(Si–OH)	1.612, 1.642	1.611	1.586
α(Si–O–Si)[a]	158.6	79.4, 96.1	
α(Si–O–Si)[b]	148.5	164.4	
r(Si–OO)	2.127	2.077	
r(O–O)	1.279	1.307	1.281

Note: Bond lengths in Å and bond angles in degrees.
[a] *cis*, next to the adsorbate $O_2^{\bullet-}$ [b] *trans*, on the opposite side to the adsorbate.

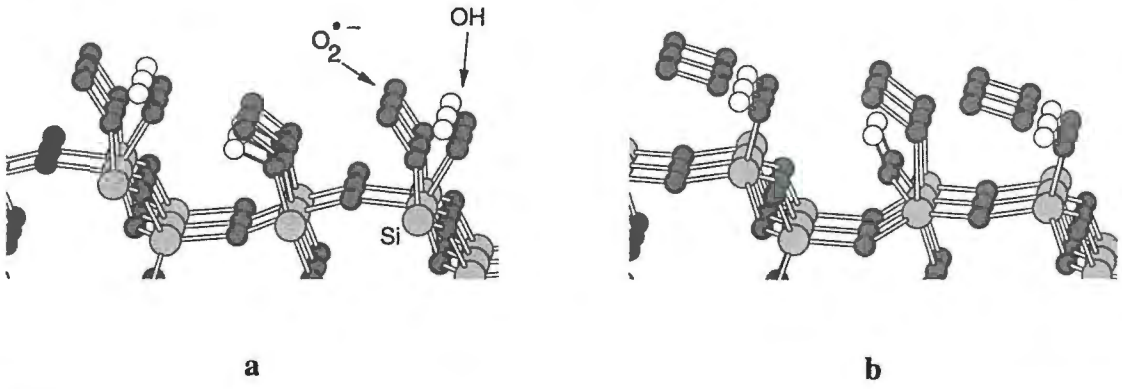

FIGURE 7. Starting (a) and optimized (b) geometry of $O_2^{\bullet -}$ adsorption product on hydroxylated (01$\bar{1}$1) α-quartz surface. One superoxide anion radical molecule is desorbed from surface during minimization, while the other remains attached to surface. Simulation performed at 1.0 monolayer coverage (i.e., one superoxide radical molecule per surface silicon atom in starting configuration).

None of the $O_2^{\bullet -}$ adsorption leads directly to subsurface Si–O bond dissociation as observed during minimization of the •OH/(01$\bar{1}$1) product. This is consistent with the cluster model prediction of a higher energy barrier for the Si–OSi bond rupture in the superoxide anion radical activated process compared to the hydroxyl radical activated surface dissolution. It is also important to note that our calculations did not include solvent effects. Solvation of negatively charged superoxide anion radicals in a polar solvent (e.g., water) may impede $O_2^{\bullet -}$ access to the surface, thus impacting the kinetics of the adsorption.

We also expect that similar adsorption mechanisms, eventually causing surface reconstruction and regeneration of surface-based radicals, are possible for other polymorphs of silica. However, the extent of these interactions will depend on the specific local geometry of the silica. On the basis of our calculations, it is not only the polymorphic type, but also the cleavage plane in which the crystal is cut, that determines the actual surface silicon atom configuration and consequently its reactivity.

It is important to note that other factors will also modulate the extent of free radical/silica surface interaction. For instance, co-adsorption of phospholipids, the major component of pulmonary surfactant, has been shown to play an important role in the overall silica toxicity mechanism.[45-49] Other adsorbents that alter either chemical or physical properties of the silica surface will similarly influence the silica surface pathogenic behavior.

Experimental Results

To test the theoretical predictions, we performed an experimental study of the ability of superoxide anion radicals to refresh aged silica surfaces (i.e., the ability to regenerate reactive silicon-based radicals on the surface). The effect of superoxide radicals on the generation of chemiluminescence (CL) by aged silica is shown in Fig. 8. Aged silica alone did not generate CL above the control (medium blank) level. The generation of superoxide by xanthine/xanthine oxidase was verified by a significant increase (46%) in CL above control. Superoxide interacted with aged silica to generate more CL than superoxide alone. This increase above superoxide alone was dependent upon the concentration of silica—that is, a 66% and 116% enhancement at 0.05 and 0.1 mg/mL silica, respectively, when expressed as a percentage of the increase due to superoxide alone. This enhancement of CL in the presence of aged silica is consistent with the refreshening of the silica surface by superoxide radicals.

The above results are consistent with the generation of siloxyl radicals from the reaction of $O_2^{\bullet -}$ with Si–O bonds of aged silica. However, an alternative explanation is feasible; that the xanthine/xanthine oxidase reaction generated H_2O_2 as well as $O_2^{\bullet -}$. This H_2O_2 could participate in a Fenton-like reaction with trace metals on the silica surface to generate •OH, which resulted in enhanced CL. Indeed, under the experimental conditions of this study, xanthine/xanthine oxidase generated 16 μM H_2O_2. However, the com-

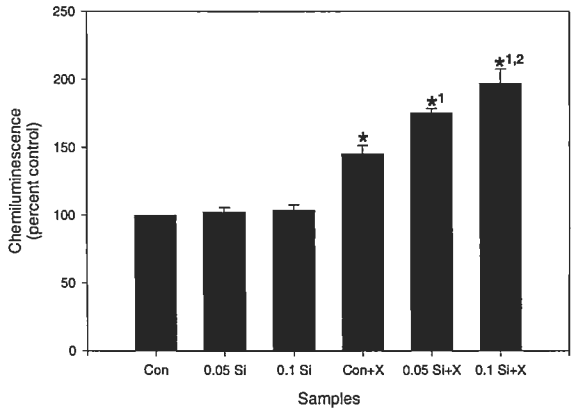

FIGURE 8. Refreshening of aged silica surface by superoxide. Freshness of silica surface determined by measuring chemiluminescence (CL) generated by silica (0.05 and 0.1 g/mL) suspended in HEPES-buffered medium containing 0.008 mg % luminol. CL measured using a luminometer at 42 °C for 45 min in absence or presence of superoxide generation system. Superoxide generated by reaction of xanthine (1 mM) and xanthine oxidase (20 μM). Con indicates medium blank; Si indicates aged silica; X indicates xanthine/xanthine oxidase; * indicates significant increase from medium blank; 1 indicates significantly greater than additive effect of X and 0.05 g/mL Si alone; 2 indicates significantly greater than additive effect of X and 0.1 g/mL Si alone.

bination of 16 μM H_2O_2 with 0.1 mg/mL silica failed to generated substantial CL. That is, this combination increased CL by 15% above the medium blank. Such an effect is far too small to account for this 116% enhancement of CL when 0.1 mg/mL silica was added to xanthine/xanthine oxidase (Fig. 8). Therefore, the data remain supportive of the refreshening of the silica surface by superoxide radicals.

Conclusions

We performed a theoretical study of the reactivity of free radicals with the hydroxylated α-quartz surface. The interaction between two biologically important radical species, hydroxyl radicals and superoxide radical anions, and the surface has been studied using two models of the surface. While the small cluster model allows for very accurate predictions of the structure and energetics of species involved in localized surface events, the more extensive 3-dimensional periodic slab model includes nonlocal and bulk effects. Two of the most energetically stable hydroxylated α-quartz cleavages were investigated—the (0001) and (01$\bar{1}$1) surfaces.

The slab model calculation confirmed an earlier prediction that •OH easily adsorbs on both the (0001) and (01$\bar{1}$1) surfaces and that the adsorption weakens the Si–O subsurface bonds. However, while the •OH/(0001) adsorption is followed by hydrogen abstraction from the surface silanol group, the •OH/(01$\bar{1}$1) adsorption leads directly to surface disintegration. This surprising result suggests that •OH adsorption on the (01$\bar{1}$1) surface destabilizes the surface to such an extent that it is immediately followed by the subsurface Si–O bond rupture and surface dissolution. This also implies that the energy barrier to the subsurface Si–O bond dissociation is very small. The product of both the •OH/(0001) and •OH/(01$\bar{1}$1) adsorption and surface reconstruction is a surface terminated by silanols and siloxyl radicals, Si–O•. Thus, although the aged, silanol terminated quartz surface is chemically quite inert, its interaction with •OH can lead to its reconstruction and transformation to a surface terminated by very reactive surface silicon-based radicals. The activated surface can then actively participate in further radical propagation reactions and eventually in deleterious interactions with adsorbed biological macromolecules and cells. This proposed reaction opens up a possible pathway for the aged quartz surface involvement in silica toxicity mechanisms.

The predicted interaction between superoxide anion radicals and the hydroxylated quartz surface is more subtle. While the $O_2^{\bullet-}$ adsorbs to some extent on both surfaces, the adsorbates are less strongly bonded to the surface. The estimated energy barrier for $O_2^{\bullet-}$ induced subsurface Si–O bond rupture is 10 kcal/mol, which is larger than for the •OH activated process (4 kcal/mol). Thus, although the reactivation of the surface by $O_2^{\bullet-}$ is predicted to be likely, it will be much more efficiently done by hydroxyl radicals.

The results of the calculations also point to the importance of the surface silicon atoms' local geometries on their adsorption properties and reactivity. Not only do these properties vary for geminal and isolated silanol sites, but also for two isolated silanol sites differing only by the surface silicon atom geometrical conformation.

The theoretical predictions are supported experimentally by monitoring the chemical re-activation of the surface and formation of surface silicon-based radicals by superoxide anion radicals using chemiluminescence.

References

1. IARC monographs on the evaluation of the carcinogenic risk of chemicals to humans: silica, some silicates, coal dust and para-aramid fibrils. Vol. 68; 1997.
2. Driscoll KE, Higgins JM, Leytart MJ, Crosby LL. Differential effects of mineral dusts on the in vivo activation of alveolar macrophage eicosanoid and cytokine release. Toxic In Vitro 1990;4:284–288.
3. Vallyathan V, Kang JH, Van Dyke K, Dalal NS, Castranova V. Response of alveolar macrophages to in vitro exposure to freshly fractured versus aged silica dust: the ability of prosil 28, an organic material, to coat silica and reduce its biological reactivity. J Toxicol Environ Health 1991;33:303–315.
4. Janssen YMW, Marsh JP, Absher MP, Hemenway D, Vacek PM, Lelie KO, Borm PJA, Mossman BT. Expression of antioxidant enzymes in rat lung after inhalation of asbestos and silica. J Biol Chem 1992;267: 10625–10630.
5. Fubini B, Bolis V, Cavenago A, Volante M. Physicochemical properties of crystalline silica dusts and their possible implication in various biological responses. Scand J Work Environ Health 1995;21 Suppl 2:9-14.
6. Castranova V, Dalal NS, Vallyathan V. Role of surface free radicals in the pathogenicity of silica. In: Castranova V, Vallyathan V, Wallace WE, editors. Silica and silica-induced lung diseases. Boca Raton FL: CRC Press; 1996: 91–105.
7. Castranova V, Antonini JM, Reasor MJ, Wu L, VanDyke K. Oxidant release from pulmonary phagocytes. In: Castranova V, Vallyathan V, Wallace WE, editors. Silica and silica-induced lung diseases. Boca Raton FL: CRC Press; 1996: 185–195.
8. Fubini B, Otero Areán C. Chemical aspects of the toxicity of inhaled mineral dusts. Chem Soc Rev 1999;28:373–381.
9. Fubini B, Bolis V, Giamello E. The surface chemistry of crushed quartz dust in relation to its pathogenicity. Inorg Chim Acta 1987;138:193–197.
10. Vallyathan V, Shi X, Dalal NS, Irr W, Castranova V. Generation of free radicals from freshly fractured silica dust. Am Rev Respir Dis 1988;138:1213–1219.
11. Fubini B, Giamello E, Volante M. The possible role of surface oxygen species in quartz pathogenicity. Inorg Chim Acta 1989;162:187–189.
12. Fubini B, Giamello E, Pugliese L, Volante M. Mechanically induced defects in quartz and their impact on pathogenicity. Solid State Ionics 1989;32/33: 334–343.
13. Fubini B, Giamello E, Volante M, Bolis V. Chemical functionalities at the silica surface determining its reactivity when inhaled. Formation and reactivity of surface radicals. Toxicol Ind Health 1990;6:571–598.
14. Costa D, Fubini B, Giamello E, Volante M. A novel type of active site at the surface of crystalline SiO_2 (α-quartz) and its possible impact on pathogenicity. Can J Chem 1991;69:1427–1434.
15. Castranova V, Pailes WH, Dalal NS, Miles PR, Bowman L, Vallyathan V, Pack D, Weber KC, Hubbs A, Schwegler-Berry D, Xiang J, Dey R, Blackford J, Ma JYC, Barger M, Shoemaker DA, Pretty JR, Ramsey DM, McLaurin JL, Khan A, Baron PA, Childress CP, Stettler LE, Teass AW. Enhanced pulmonary response to the inhalation of freshly fractured silica as compared with aged dust exposure. Appl Occup Environ Hyg 1996;11:937–941.
16. Elias Z, Poirot O, Daniére MC, Terzetti F, Marande AM, Dzwigaj S, Pezerat H, Fenoglio I, Fubini B. Cytotoxic and transforming effects of silica particles with different surface properties in Syrian hamster embryo (SHE) cells. Toxic In Vitro 2000;14: 409–422.
17. Guthrie GD Jr, Heaney PJ. Mineralogical characteristics of silica polymorphs in relation to their biological activities. Scand J Work Environ Health 1995;21 Suppl. 2:5–8.
18. Zalma R, Bonneau L, Jaurand MC, Guignard J, Pezerat H. Formation of oxy radicals by oxygen reduction arising from the surface-activity of asbestos. Can J Chem 1987;652:2338–2341.
19. Pezerat H, Zalma R, Guignard J, Jaurand MC. Production of oxygen radicals by the reduction of oxygen arising from the surface activity of mineral fibers. In: Bignon J, Peto J, Saracci R, editors. Non-occupational exposure to mineral fibres, IARC, Lyon, France, IARC Scientific Publications 90; 1989: 100–110.
20. Pezerat H. The surface activity of mineral dusts and the process of oxidative stress. In: Brown RC, Hoskins JA, Johnson NF, editors. Mechanisms in fiber carcinogenesis, NATO ASI Series. New York: Plenum Publishing; 1991: 387–395.
21. Shoemaker DA, Pretty JR, Ramsey DM, McLaurin JL, Khan A, Teass AW, Castranova V, Pailes WH, Dalal NS, Miles PR, Bowman L, Leonard S, Shumaker J, Vallyathan V, Pack D. Particle activity and in vivo pulmonary response to freshly milled and aged alpha-quartz. Scand J Work Environ Health 1995;21 Suppl. 2:15–18.
22. Costa D, Guignard J, Pezerat H, Fubini B. Reactivité de surface des silices vis a vis de l'oxigène et de l`eau oxigénée dans la production de radicaux OH. Relations possibles avec la fibrogénèse. In: Sebastien P, editor. Mechanisms in occupational lung diseases, Vol. 203, Colloque INSERM; 1991, 311–316.

23. Konecny R. Reactivity of hydroxyl radicals on hydroxylated quartz surfaces: I. Cluster model calculations. J Phys Chem B 2001;105:6221–6226.
24. Xiao Y, Lasaga AC. *Ab initio* quantum mechanical studies of the kinetics and mechanism of quartz dissolution: OH^- catalysis. Geochim Cosmochim Acta 1996;60:2283–2295.
25. Sneh O, George SM. Thermal stability of hydroxyl groups on a well-defined silica surface. J Phys Chem 1995;99:4639–4647.
26. Chuang I, Maciel GE. Probing hydrogen bonding and the local environment of silanols on silica surfaces via nuclear spin cross polarization dynamics. J Am Chem Soc 1996;118:401–406.
27. Chuang I, Maciel GE. A detailed model of local structure and silanol hydrogen bonding of silica gel surfaces. J Phys Chem B 1997;101:3052–3064.
28. Lee C, Yang W, Parr RG. Development of the Colle-Salvetti correlation-energy formula into a functional of the electron density. Phys Rev B 1988;37:785–789.
29. Becke AD. A new mixing of Hartree-Fock and local density-functional theories. J Chem Phys 1993;98: 1372–1377.
30. Schlegel HB. Optimization of equilibrium geometries and transition structures. J Comput Chem 1982;3: 214–218.
31. Frisch MJ, Trucks GW, Schlegel HB, Scuseria GE, Stratmann RE, Burant JC, Dapprich S, Millam JM, Daniels AD, Kudin KN, Strain MC, Farkas O, Tomasi J, Barone V, Cossi M, Cammi R, Mennucci B, Pomelli C, Adamo C, Clifford S, Ochterski J, Cui Q, Morokuma K, Malick DK, Rabuck AD, Liu G, Liashenko A, Piskorz P, Komaromi I, Gill PMW, Johnson BG, Robb MA, Cheeseman JR, Keith TA, Petersson GA, Montgomery JA, Raghavachari K, Al-Laham MA, Zakrzewski VG, Ortiz JV, Foresman JB, Cioslowski J, Stefanov BB, Nanayakkara A, Challacombe M, Peng CY, Ayala PY, Chen W, Wong MW, Andres JL, Replogle ES, Gomperts R, Martin RL, Fox DJ, Head-Gordon M, Gonzales C, Pople JA. Gaussian 98 (Revision A.7). Pittsburgh, PA: Gaussian, Inc; 1998.
32. Kresse G, Hafner J. Ab-initio molecular dynamics for open-shell transition metals. Phys Rev B 1993;48: 13115–13118.
33. Kresse G, Hafner J. Ab-initio molecular-dynamics simulation of the liquid-metal amorphous-semiconductor transition in germanium. Phys Rev B 1994;49: 14251–14269.
34. Kresse G, Furthmüller J. Efficiency of ab-initio total energy calculations for metals and semiconductors using a plane-wave basis set. Comput Mater Sci 1996;6:15–50.
35. Kresse G, Furthmüller J. Efficient iterative schemes for *ab initio* total-energy calculations using a plane-wave basis set. Phys Rev B 1996;54:11196–11186.
36. Hohenberg P, Kohn W. Inhomogeneous electron gas. Phys Rev B 1964;136:864–871.
37. Kohn W, Sham L. Self-consistent equations including exchange and correlation effects. Phys Rev A 1965;140:1133–1138.
38. Vanderbilt D. Soft self-consistent pseudopotentials in a generalized eigenvalue formalism. Phys Rev B 1990;41:7892–7895.
39. Kresse G, Hafner J. Norm-conserving and ultrasoft pseudopotentials for first-row and transition-elements. J Phys Condens Matter 1994;6:8245–8257.
40. Monkhorst HJ, Pack JD. Special points for brillouin-zone integrations. Phys Rev B 1976;13: 5188–5192.
41. Jepsen O, Andersen OK. The electronic structure of hcp ytterbium. Solid State Commun 1991;9:1763–1767.
42. Blöchl P, Jepsen O, Andersen OK. Improved tetrahedron method for brillouin-zone integrations. Phys Rev B 1994;49:16223–16233.
43. Castranova V, Vallyathan V, Van Dyke K, Dalal NS. Use of chemiluminescence assays to monitor the surface characteristics and biological reactivity of freshly fractured vs aged silica. In: Mossman BT, Bégin RO, editors. Effects of mineral dusts on cells. Vol. H30 NATO ASI Series. Berlin: Springer-Verlag; 1989: 181–188.
44. March J. Advanced organic chemistry. 3rd ed. New York: Wiley; 1985: 609.
45. Wallace WE, Keane MJ, Mike PS, Hill CA, Vallyathan V, Regad ED. Contrasting respirable quartz and kaolin retention of lecithin surfactant and expression of membranolytic activity following phospholipase A_2 digestion. J Toxicol Environ Health 1992;37:391–409.
46. Hill CA, Wallace WE, Keane MJ, Mike P. The enzymatic removal of a surfactant coating from quartz and kaolin by P388D1 cells. Cell Biol Toxicol 1995; 11:119–128.
47. Wallace WE, Keane MJ, Harrison JC, Stephens JW, Brower PS, Grayson RL, Attfield MD. Surface properties of silica in mixed dusts. In: Castranova V, Vallyathan V, Wallace WE, editors. Silica and silica-induced lung diseases. Boca Raton FL: CRC Press; 1996: 107–117.
48. Keane MJ, Wallace WE. Pulmonary surfactant adsorption and the expression of silica toxicity. In: Castranova V, Vallyathan V, Wallace WE, editors. Silica and silica-induced lung diseases. Boca Raton FL: CRC Press; 1996: 271–281.
49. Fubini B, Wallace WE. Modulation of silica pathogenicity by surface processes. In: Papirer E, editor. Adsorption on silica surfaces. New York: Marcel Dekker; 2000: 645–664.